J Comput Neurosci
DOI 10.1007/s10827-008-0112-8

Loss of phase-locking in non-weakly coupled inhibitory networks of type-I model neurons

Myongkeun Oh · Victor Matveev

Received: 19 November 2007 / Revised: 4 July 2008 / Accepted: 9 July 2008

Abstract Synchronization of excitable cells coupled by reciprocal inhibition is a topic of significant interest due to the important role that inhibitory synaptic interaction plays in the generation and regulation of coherent rhythmic activity in a variety of neural systems. While recent work revealed the synchronizing influence of inhibitory coupling on the dynamics of many networks, it is known that strong coupling can destabilize phase-locked firing. Here we examine the loss of synchrony caused by an increase in inhibitory coupling in networks of type-I Morris–Lecar model oscillators, which is characterized by a period-doubling cascade and leads to mode-locked states with alternation in the firing order of the two cells, as reported recently by Maran and Canavier (J Comput Nerosci, 2008) for a network of Wang-Buzsáki model neurons. Although alternating-order firing has been previously reported as a near-synchronous state, we show that the stable phase difference between the spikes of the two Morris–Lecar cells can constitute as much as 70% of the unperturbed oscillation period. Further, we examine the generality of this phenomenon for a class of type-I oscillators that are close to their excitation thresholds, and provide an intuitive geometric description of such "leap-frog" dynamics. In the Morris–Lecar model network, the alternation in the firing order arises under the condition of fast closing of K^+ channels at hyperpolarized potentials, which leads to slow dynamics of membrane potential upon synaptic inhibition, allowing the presynaptic cell to advance past the postsynaptic cell in each cycle of the oscillation. Further, we show that non-zero synaptic decay time is crucial for the existence of leap-frog firing in networks of phase oscillators. However, we demonstrate that leap-frog spiking can also be obtained in *pulse-coupled* inhibitory networks of one-dimensional oscillators with a multi-branched phase domain, for instance in a network of quadratic integrate-and-fire model cells. Finally, for the case of a homogeneous network, we establish quantitative conditions on the phase resetting properties of each cell necessary for stable alternating-order spiking, complementing the analysis of Goel and Ermentrout (Physica D 163:191–216, 2002) of the order-preserving phase transition map.

Keywords Synchronization · Non-weak coupling · Non-synchronous dynamics · Inhibitory network · Type-I excitability · Synaptic inhibition · Leader switching · Spike-time response · Phase resetting

Action Editor: Frances K. Skinner

Electronic supplementary material The online version of this article (doi:10.1007/s10827-008-0112-8) contains supplementary material, which is available to authorized users.

M. Oh · V. Matveev (✉)
Department of Mathematical Sciences
and Center for Applied Mathematics and Statistics,
New Jersey Institute of Technology,
Newark, NJ 07102, USA
e-mail: matveev@njit.edu

1 Introduction

The question of synchronization of coupled oscillators is of fundamental importance for the understanding of rhythmogenesis in biological networks, and has been a subject of great interest in mathematical biology

and neuroscience (Winfree 2001; Izhikevich 2006). In order to better understand the dynamics of multi-neuron networks, it is important to fully examine the case of a two-cell network, particularly relevant in the study of central pattern generators which often contain sub-circuits composed of pairs of mutually inhibitory cells. When the coupling between oscillators is weak, synchronization and its stability can be analyzed using the well-developed geometric phase-reduction approach and the method of averaging (Kuramoto 1984; Ermentrout and Kopell 1984, 1990; Hoppensteadt and Izhikevich 1997; Izhikevich and Kuramoto 2006). The weak-coupling theory is very general in its applicability, and for a homogeneous two-cell network predicts stable phased-locked firing, either synchronous or anti-synchronous, depending on the properties of the coupling and the intrinsic dynamics of the oscillators (van Vreeswijk et al. 1994; Hansel et al. 1995; Ermentrout 1996). Non-weakly coupled networks can exhibit a much richer variety of dynamic behaviors, but their analysis presents a much greater challenge, as there is no general method of determining the stable modes of network activity in this case. However, in the case of pulsatile coupling which is lasting only briefly relative to the length of the unperturbed period, and in the case of sufficiently fast return to the limit cycle upon synaptic perturbation, the dynamics of non-weakly coupled networks can be analyzed using Poincaré return maps for the inter-spike intervals, derived from the phase-resetting curves of the coupled cells (Winfree 2001; Kopell 1988; Canavier et al. 1999; Goel and Ermentrout 2002; Jones et al. 2000; Kopell et al. 2000; Kopell and Ermentrout 2002; Acker et al. 2003). The Poincaré firing map approach is also useful in the analysis of non-weakly coupled relaxation oscillators (Somers and Kopell 1993; Rubin and Terman 2000; Izhikevich 2000), and for networks of one-dimensional model cells such as integrate-and-fire units (Mirollo and Strogatz 1990; van Vreeswijk et al. 1994; Bressloff and Coombes 2000).

While recent work has revealed the synchronizing role of inhibitory synaptic interaction on the activity of many networks (reviewed in White et al. 1998), it is known that non-weak coupling can destabilize phase-locked dynamics (Ermentrout and Kopell 1991). For instance, many network models exhibit the transition to the "oscillator death" mode as the coupling strength is increased, whereby some of the neurons become trapped at a fixed point by the strong synaptic currents arriving from the active cell (Ermentrout and Kopell 1990; Bressloff and Coombes 1998). Further, several recent studies explored the emergence of more complex non phase-locked states in the case of heterogeneous networks, whereby both neurons are active at different intervals of the oscillation period (see e.g. White et al. 1998; Bressloff and Coombes 2000). In

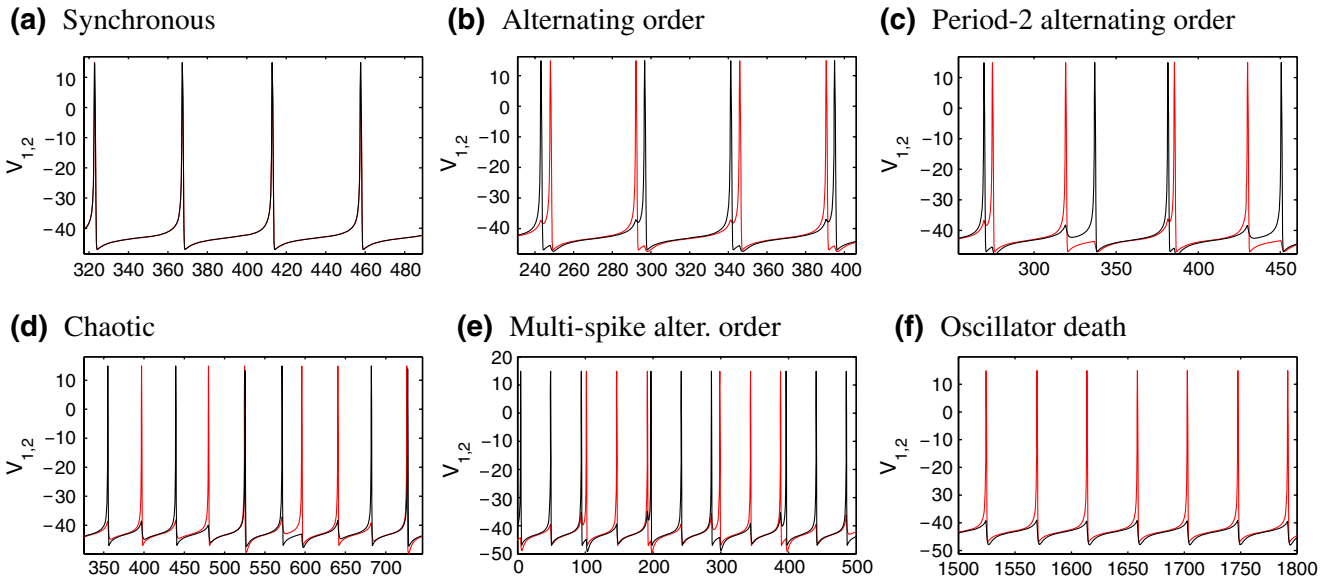

Fig. 1 Network activity states at different values of coupling strength, $\bar{g}_{syn}$. The potentials of the two cells are shown as red and black traces, respectively. (**a**) Synchronous phase-locked firing ($\bar{g}_{syn} = 0.03$). The spiking period is close to the unperturbed period of 45 ms. (**b**) Alternating-order (leap-frog) spiking ($\bar{g}_{syn} = 0.17$) (**c**) Period-2 alternating-order spiking ($\bar{g}_{syn} = 0.22$) (**d**) Chaotic state, irregular inter-spike intervals ($\bar{g}_{syn} = 0.29$) (**e**) Bursting (3:3 alternating-order firing, $\bar{g}_{syn} = 0.34$) (**f**) Spike-suppress state ("oscillator death", $\bar{g}_{syn} = 0.5$)

particular, recent work of Maran and Canavier (2008) revealed that the assumption of preserved firing order does not hold in a network of Wang-Buzsáki model neurons with type-I excitability (Wang and Buzsáki 1996). They showed the emergence of 2:2 mode-locked states (see Fig. 1(b), (c)), and examined the influence of heterogeneity and second-order phase resetting on this network activity state.

The goal of our work is to reveal the generality of such alternating-order firing (termed "leap-frog" spiking by G.B. Ermentrout, or "leader switching" by Acker et al. 2003) for inhibitory networks of type-I oscillators. In particular, we examine leap-frog dynamics observed in a network of simpler Morris–Lecar model neurons in a parameter regime corresponding to type-I excitability. This network exhibits synchronous firing for weak coupling, which is readily destabilized even by a moderate increase in coupling strength (Figs. 1, 2). Our aim is to provide an intuitive geometric description of this activity state, by examining the features of the phase-space trajectory of the two cells during spike-order switching. We show that leap-frog dynamics can arise in inhibitory networks of cells which are close to their excitation thresholds, under the additional condition of slow dynamics of membrane potential upon hyperpolarization. In the Morris–Lecar model we consider, such slow dynamics is caused by the fast closing of K^+ channels at hyperpolarized potentials, which leads to time-scale separation and associated trapping of the trajectory by the nullcline of the recovery variable. This allows even a moderate synaptic inhibition to retard the dynamics of the postsynaptic cell for a duration which is greater than the interval since the preceding spike of that cell, leading to the change of the spiking order.

An interesting aspect of the alternating-order spiking is that it cannot be obtained in a network of phase oscillators with instantaneous synaptic coupling, and that non-zero synaptic time constant is crucial for achieving leap-frog spiking in such networks. However, we show that order alternation can be obtained in a purely *pulse-coupled* network if the phase domain of each oscillator is augmented with an additional negative-value branch representing the strong suppression of the cell upon synaptic inhibition. For instance, we find that leap-frog spiking can also be achieved in a network of pulse-coupled quadratic integrate-and-fire model neurons. Further, such pulse-coupled augmented phase model network provides an accurate description for the dynamics of the Morris–Lecar model network. Following Maran and Canavier (2008), we use the phase-resetting method to analyze leap-frog spiking on a quantitative level, and provide a simplified analysis of existence and stability conditions for leap-frog spiking for the case of identical cells. Restricting our consideration to a homogeneous network allows us to establish the most basic conditions on the phase-resetting properties necessary for leap-frog spiking.

We note that alternating-order firing was examined previously in homogeneous networks of two coupled relaxation oscillators with excitatory synapses by Bose et al. (2000) and with inhibitory synapses by Sato and Shiino (2007). However, in both works the stable phase difference between successive spikes of the two cells is much smaller than the width of an action potential. This is also true for the activity states explored by Maran and Canavier (2008). For this reason, earlier studies referred to the alternating-order spiking as a near-synchronous state. In contrast, here we show that

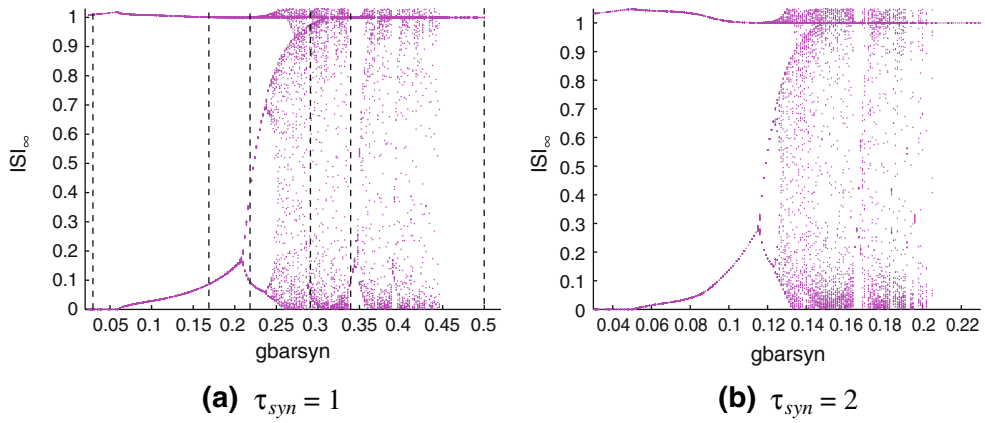

Fig. 2 Bifurcation diagram of the Morris–Lecar model network. ISI_∞, the asymptotic values of the intervals between consecutive spikes (not necessarily spikes of the same cell) are plotted as a function of the coupling strength, $\bar{g}_{syn}$, for two values of synaptic decay time: (**a**) $\tau_{syn} = 1$ and (**b**) $\tau_{syn} = 2$. The *dotted lines* correspond to each of the six activity states in Fig. 1(a)-(f). Note the difference in scale along the $\bar{g}_{syn}$ axis

the interval between the neighboring spikes of the two cells can constitute more than one half of the resting oscillation period. This is particularly true for the multiple-period leap-frog spiking, in which case the interval between the spikes of the two cells can reach 70% of the unperturbed period, and is an order of magnitude longer than the decay time of synaptic inhibition (see e.g. Fig. 1(c)). Thus, alternating-order activity represents a distinct activity state that cannot be described as a near-synchronous state.

2 Model

We consider a pair of two identical model neurons with type-I excitability (Rinzel and Ermentrout 1998), each modeled as a Morris–Lecar oscillator (Morris and Lecar 1981). Each cell possesses a periodic limit cycle trajectory corresponding to an action potential, which results from the interplay between the depolarizing calcium current I_{Ca} and the activation w of the repolarizing potassium current, I_K. The two cells are assumed to be identical, and are coupled by an inhibitory synaptic current, $I_{syn}(V,s)$:

$$\begin{aligned} C\frac{dV}{dt} &= -I_{Ca} - I_K - I_L - I_{syn}(V,s) - I_{app} \\ \frac{dw}{dt} &= (w_\infty(V) - w)/\tau_\infty(V) \\ I_{Ca} &= \bar{g}_{Ca} m_\infty(V)(V - V_{Ca}) \\ I_K &= \bar{g}_K w(V)(V - V_K) \\ I_L &= \bar{g}_L(V - V_L) \end{aligned} \tag{1}$$

where $C = 2\ \mu F/cm^2$ is the membrane capacitance, V is the cell membrane voltage in mV, t is time in ms, I_L is the passive leak current, and $I_{app} = -14\ \mu$A/cm^2 is the applied current. The remaining parameters are $V_{Ca} =$ 120mV, $V_K = -84$mV, $V_L = -60$mV, $g_{Ca} = 4$mS/cm^2, $g_K = 8$mS/cm^2, $g_L = 2$mS/cm^2.

The steady-state activation of calcium current is

$$m_\infty(V) = \frac{1}{2}\left[1 + \tanh\left(\frac{V+12}{18}\right)\right]$$

The potassium current activation amplitude and activation rate are

$$\begin{aligned} w_\infty(V) &= \frac{1}{2}\left[1 + \tanh\left(\frac{V+8}{6}\right)\right] \\ \frac{1}{\tau_\infty(V)} &= \frac{2}{3}\cosh\left[\frac{V+8}{12}\right] \end{aligned} \tag{2}$$

Given this choice of model parameters, each of the two uncoupled oscillators exhibits periodic spiking with a period of about 45 ms. Note the fast approach of $\tau_w(V)$ to zero at hyperpolarized potentials (Eq. (2)), whereby the trajectory overlaps the w-nullcline in the quiescent phase of the oscillation (see schematic representation of the limit cycle in Fig. 4). The fast closing of the K^+ channels is a critical condition for achieving alternating-order spiking in the Morris–Lecar model. Such fast kinetics of the w variable can be somewhat relaxed without destroying the qualitative aspects of the dynamics, and alternating-order firing can also be achieved in the type-I parameter regime corresponding to Fig. 7.7 of Rinzel and Ermentrout (1998).

The two cells are coupled through the synaptic current given by

$$I_{syn} = \bar{g}_{syn} s(t)(V - V_{inh})$$

where $\bar{g}_{syn}$ is the maximum synaptic conductance and $V_{inh} = -80$ mV is the reversal potential. The dynamics of the synaptic gating variable $s(t)$ depends on the presynaptic cell potential, V_{pre}:

$$\frac{ds}{dt} = -\frac{s}{\tau_{syn}}\sigma(V_{th} - V_{pre}) + \frac{1-s}{\tau_\gamma}\sigma(V_{pre} - V_{th}) \tag{3}$$

where $V_{th} = -3$ mV is the synaptic threshold, $\sigma(\cdot)$ is a sigmoid function, $\sigma(x) = [1 + \tanh(4x)]/2$, and τ_{syn} and $\tau_\gamma = 0.2$ ms are the synaptic decay and rising time constants, respectively. We focus primarily on short synaptic decay times of about $\tau_{syn} = 1 - 5$ ms, and in Section 3.8 discuss the effect of longer τ_{syn}.

3 Results

3.1 Network activity states

We start by exploring in detail the behavior of the system described by Eq. (1), the two identical ML model neurons with mutually inhibitory synaptic interaction. Figure 1 shows the diversity of behaviors exhibited by this network for different values of the maximal synaptic conductance, $\bar{g}_{syn}$, and the bifurcation diagram presented in Fig. 2 demonstrates the transitions between the different activity states. For very small values of this coupling parameter, the two neurons fire in synchrony, as predicted by the weak coupling theory. When $\bar{g}_{syn}$ is increased, the synchronized state loses stability, and the network transitions to the alternating-order 2:2 mode-locked state shown in Fig. 1(b), also referred to as "leap-frog" spiking by Maran and Canavier (2008). In this state, there is a stable non-zero time interval between the spikes of the two cells, with cells changing firing order in each cycle of the oscillation.

For yet higher values of the coupling, the interval between consecutive spikes of the two cells alternates in each cycle between two distinct values, as shown in Fig. 1(c). For higher still values of $\bar{g}_{syn}$, the alternating-order firing state undergoes a period-doubling cascade and gives way to chaotic firing in which the inter-spike intervals and the spiking order change irregularly. Further, for narrow ranges of $\bar{g}_{syn}$ values multi-spike $m:n$ alternating order firing states emerge, as shown in Fig. 1(e), which represent a form of bursting. Finally, very strong coupling leads to the so-called "oscillator death" state shown in Fig. 1(f), whereby the spiking of one neuron provides enough inhibition to completely prevent the spiking of the partner cell (Ermentrout and Kopell 1990; Bressloff and Coombes 1998).

Bifurcation diagram presented in Fig. 2 explores the transitions between these different behaviors, showing the coupling-strength dependence of the asymptotic (equilibrium) intervals between two consecutive network spikes, which may or may not be the spikes of the same cell. These inter-spike intervals are normalized to the period of the uncoupled cell, and are denoted ISI_∞. The values of $\bar{g}_{syn}$ corresponding to each of the activity states shown in Fig. 1 are marked by vertical dashed lines. Even though the set of ISI_∞ values does not fully characterize the network state, since it does not explicitly contain information about the spiking order of the two cells, it allows one to easily infer the dynamics at any given value of $\bar{g}_{syn}$. Note in particular that the presence of the value $ISI_\infty \approx 1$ indicates that at least one of the cells spikes twice in a row in each cycle, with negligible interference from the other cell. This is only possible if the cells change their firing order in each oscillation cycle. The fact that the interval between the spikes of the same cell in Fig. 1(b)–(c) is close to the unperturbed period indicates that the second-order phase resetting is not crucial for the alternating order state, and that the first-order phase resetting dominates (cf. Maran and Canavier 2008). It is one of our main goals to provide a simple geometric explanation and quantitative analysis of the alternating-order spiking behavior seen in Fig. 1(b)–(c), and to explain the period-doubling cascade evident in Fig. 2.

Figure 2(b) presents the bifurcation diagram for a larger value of the synaptic decay time constant ($\tau_{syn}=2$ as opposed to $\tau_{syn}=1$ used in all the simulations in this paper), and demonstrates that the qualitative features of the network behavior are preserved for a range of τ_{syn} values. The main effect of prolonging synaptic decay is to increase the total amount of inhibition that each cell receives from its partner, thereby compressing the bifurcation diagram along the $\bar{g}_{syn}$ axis. The dynamics of the network undergoes a significant change only for values of τ_{syn} beyond about 6 ms, or roughly 1/8 of the unperturbed period of 45 ms. The case of longer synaptic decay time is examined in Section 3.8.

3.2 Destabilization of phase-locked firing: comparison of excitation and inhibition

Given the type-I Morris–Lecar parameter regime we consider, the weak coupling theory predicts stable anti-synchronous and synchronous firing for excitatory and inhibitory synaptic coupling, respectively (van Vreeswijk et al. 1994; Hansel et al. 1995; Ermentrout 1996). As demonstrated in Fig. 3, this agrees with the dynamics exhibited by our model in the case of small synaptic conductance (top panels, $\bar{g}_{syn}=0.01$). As the synaptic conductance is increased however, there is a qualitative difference between the stability of phase-locked firing in the case of excitation versus inhibition.

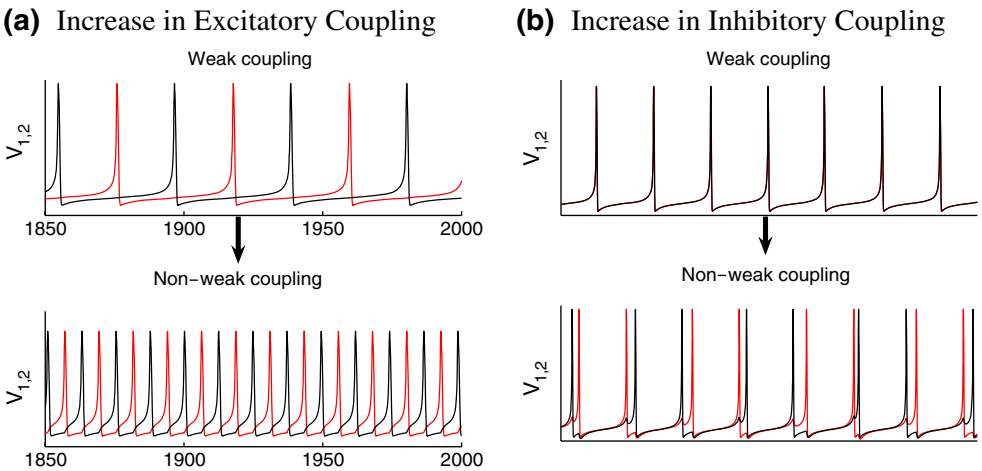

Fig. 3 Effect of an increase in coupling strength on the stability of phase-locked firing in (**a**) an excitatory network, and (**b**) an inhibitory network. $\bar{g}_{syn}$ changes from 0.01 to 0.2 in both cases. In the case of excitation (**a**), anti-phase synchronous firing is stable for a wide range of coupling strength, while the phase-locked synchronous firing is readily destabilized in the case of mutual inhibition (**b**)

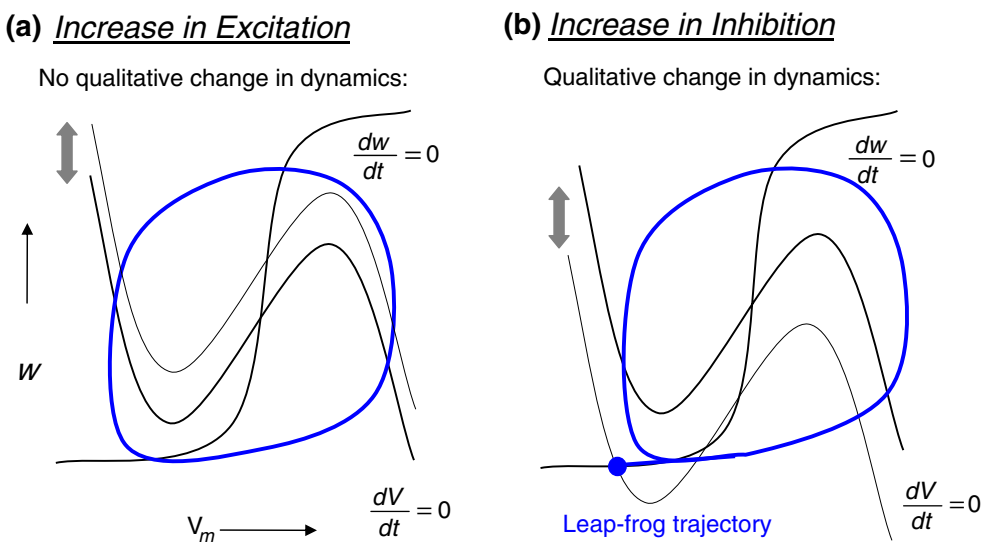

Fig. 4 Effect of non-weak coupling on the phase-plane trajectory of the postsynaptic cell. Double arrows indicate the movement of the V-nullcline during each cycle of the network oscillation. (**a**) In the case of excitation, an increase in synaptic coupling causes no qualitative change in the phase-plane dynamics. (**b**) For sufficiently strong inhibition, the V-nullcline of the post-synaptic cell intersects the w-nullcline with each presynaptic input, pushing the cell below the excitation threshold and off the limit cycle trajectory. *Thick blue curve* indicates the trajectory of each cell during one cycle of the alternating-order spiking shown in Fig. 1(b), (c). Note that the trajectory overlaps the w-nullcline during the hyperpolarized phase of the oscillation

Namely, the anti-synchronous state remains stable for non-weak excitatory coupling (see Fig. 3(a)), but an increase in inhibitory coupling quickly destabilizes phase-locking and leads to the alternating-order state shown in Fig. 3(b).

This difference between the effects of non-weak excitation and inhibition becomes obvious when one considers the phase plane dynamics of the system. Figure 4 illustrates schematically the effect of non-weak synaptic interaction on the phase-plane dynamics of the post-synaptic cell. Note that there is no qualitative change in the geometry for a wide range of excitatory conductances. However, an obvious qualitative change occurs when the inhibition strength becomes sufficiently strong to suppress the cell below its excitation through the saddle-node on the invariant cycle bifurcation (Hoppensteadt and Izhikevich 1997). If such suppression last for the entire period of the oscillation, the oscillator death occurs ("spike-suppress" state, Fig. 1(f)). However, for intermediate strength of inhibitory coupling, the suppression occurs only for part of the oscillation period, resulting in a transient subthreshold trapping of each cell during each cycle of the oscillation. This may lead to the alternation of the firing order (Fig. 1(b),(c)), whereby one cell is able to bypass its partner cell along the limit cycle by transiently keeping the other cell in the subthreshold "tail" branch of the trajectory, as depicted in Fig. 5(a). Therefore, synchrony in networks of type-I oscillators can be destabilized even for moderate increase in inhibitory coupling.

Interestingly, we find that in the Morris–Lecar model network we consider, this leader-switch mechanism remains valid even in the limit of infinitely short synaptic current. This is the result of a fast approach of the trajectory to the w-nullcline at hyperpolarized potentials, as shown in Figs. 4(b) and 5(b), which leads to the separation of time scales, with slow dynamics in the V direction, whereby the w-nullcline plays the role of the slow manifold of the system. A perturbation of sufficient strength along the slow manifold (the w-nullcine) allows to achieve a strong time delay which is longer than the time to the preceding spike. This condition is crucial for achieving leader-switching for infinitesimally short synaptic interaction. Such strong reset corresponds to an isochron that curls around the limit cycle, intersecting it at a position that is retrograde to the peak of the action potential, as shown in Fig. 5(b) (cf. discussion in Brown et al. 2004). This dynamical feature is closely linked to the cell's characteristic phase-resetting properties and the concept of negative phase, explored in the following sections.

The mechanism described above has some generality and is not specific to the Morris–Lecar model cells that we consider. In particular, we believe that the same mechanism is at play in the network of Wang-

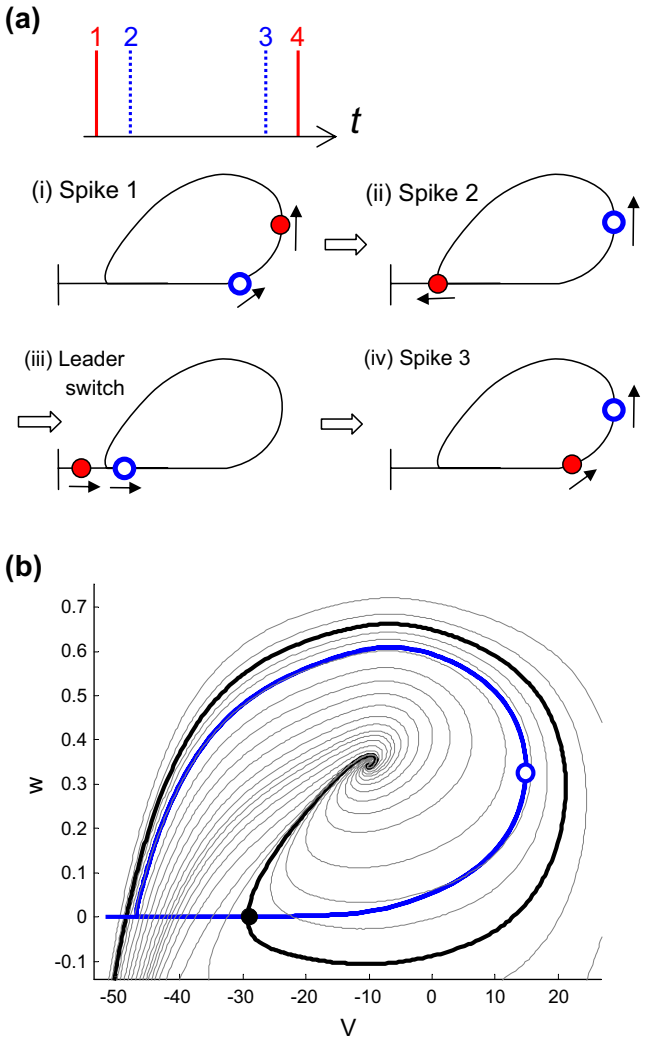

Fig. 5 Phase-plane dynamics of the coupled Morris–Lecar model cells during periodic alternating-order spiking. (**a**) Tadpole-shaped curves represent the phase-plane trajectory in panel (**b**), schematically shown in Fig. 4(b). The sequence of *four panels* describes the leap-frog spike sequence at the top, with *filled red* and *open blue circles* representing the two cells: *(i)* "red" cell spikes; *(ii)* "blue" cell spikes, pushing the "red" cell into the subthreshold branch of the trajectory (tadpole tail); *(iii)* "blue" cell bypasses the "red" cell along the unperturbed limit cycle trajectory; *(iv)* "blue" cell spikes again. The process then repeats itself, with the "red" cell emitting the next spike. (**b**) Isochron foliation of the limit cycle neighborhood. *Thick blue curve* labels the leap-frog trajectory, which partially overlaps the w-nullcline (not shown) at hyperpolarized values of potential. Note that an isochron corresponding to the hyperpolarized portion of the trajectory may intersect the limit cycle at a position (*filled circle*) which is retrograde to the peak of the preceding action potential (*open circle*)

Buzsáki oscillators (Wang and Buzsáki 1996) studied by Maran and Canavier (2008). However, the existence and stability of this dynamical state must require certain conditions on the phase-resetting properties of the cells (implicitly described by the isochron pattern of Fig. 5(b)), which will be established in Section 3.4.

3.3 Phase-reduced descriptions

Before we analyze the observed leap-frog spiking transition on a quantitative level in the next subsection, let us explore qualitatively the conditions required for the existence of this activity state. In particular, it is instructive to examine whether leap-frog firing can be obtained using a phase-reduced description of the coupled oscillators, with two phase variables ϕ_1 and ϕ_2 describing the position of each of the two cells along their unperturbed limit cycles. Note that this phase description is only possible in the weak-coupling limit, whereby the cells stay close to the limit cycle trajectory, and the phase value can be defined using the isochron foliation of its basin of attraction (Winfree 2001; Izhikevich and Kuramoto 2006). Figure 6(a) schematically illustrates the phase plane trajectory of the 2:2 periodic alternating-order firing state in terms of the corresponding (ϕ_1, ϕ_2) variables in such a general phase-reduced description, not necessarily corresponding to the specific ML network that we examine. Here the right and top boundary values ($\phi_{1,2} = 1$) correspond to the peak of an action potential of the respective cell. In the case of continuous synaptic interaction, the periodic trajectory is a continuous closed curve on the (ϕ_1, ϕ_2) torus, and its curvature is a measure of synaptic current that deflects the trajectory from a straight line. Note that the trajectory would have to self-intersect on the 2-D surface of the torus in order for the cell spike order to change in each cycle of the oscillation. Therefore, the network exhibiting alternating-order firing cannot be described in terms of autonomous flow on the (ϕ_1, ϕ_2) torus. In particular, it cannot be obtained in the framework of the weak-coupling theory, which reduces network dynamics to such an autonomous flow (reviewed in Hoppensteadt and Izhikevich 1997; Rinzel and Ermentrout 1998; Izhikevich and Kuramoto 2006):

$$\begin{aligned} \dot{\phi}_1 &= 1 + \epsilon H_{12}(\phi_2 - \phi_1) \\ \dot{\phi}_2 &= 1 + \epsilon H_{21}(\phi_1 - \phi_2) \end{aligned} \tag{4}$$

Here $H(\phi)$ is the connection function that quantifies the weak synaptic interaction, averaging it out over one oscillation period. In the case of leap-frog spiking, this averaging cannot be performed since the phase perturbation in each cycle is not an infinitesimal quantity relative to the unperturbed oscillation period. The

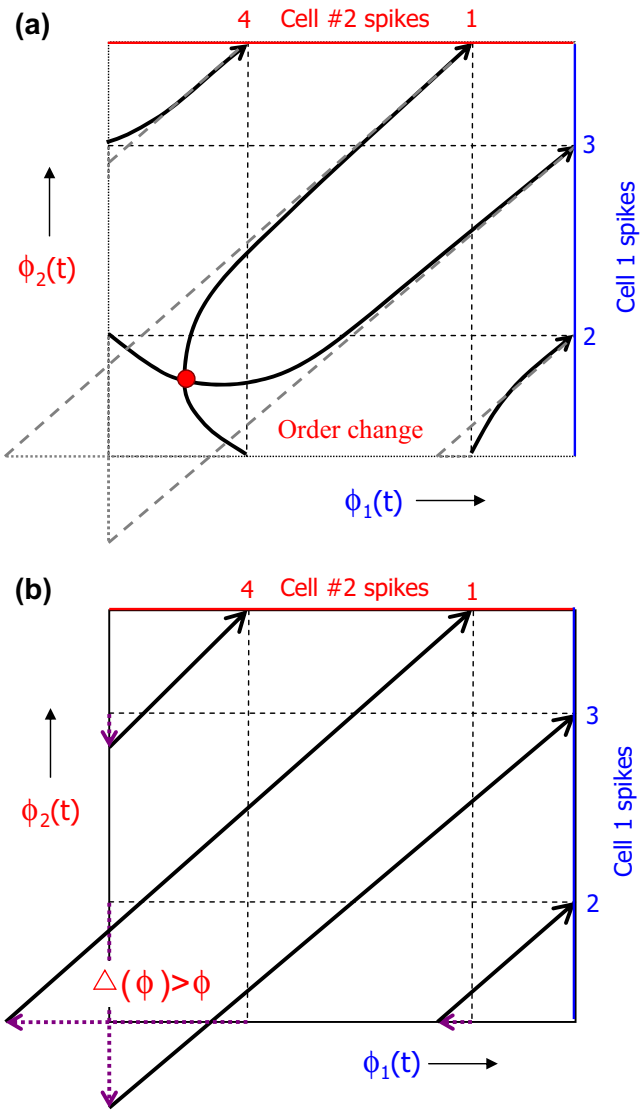

Fig. 6 Reduced phase description of the alternating-order state. (**a**) In the model with continuous synaptic interaction, the alternating-order state describes a continuous trajectory on the 2-torus. The spike times of the two cells correspond to the intersections of the trajectory with the $\phi_1 = 1$ and the $\phi_2 = 1$ boundaries, respectively. The change in spiking order requires the trajectory to self-intersect. The *dashed gray lines* indicate the correspondence between the continuous coupling description and the pulse-coupled model description shown in (**b**). In (**b**), the spike of cell i ($\phi_i = 1$) causes a discontinuous drop (*dashed arrow*) in the phase of the partner cell j by amount $\Delta(\phi_j)$, where $\Delta(\phi)$ is the spike-time response characteristic of the cell, defined to be positive in case of a phase delay. The change in firing order requires the phase domain to be augmented with an additional negative value branch. In order for the spiking order to change, the spike-triggered phase delay $\Delta(\phi)$ should be greater than current phase ϕ during the first spike that a cell receives in one cycle of the oscillation

non-existence of alternating-order firing in a network of phase oscillators is a corollary of a more general theorem of Golubitsky et al. (2006).

However, the phase topology of Fig. 6(a) provides an entirely valid description of the 2:2 activity state if it is viewed as a projection of a higher-dimensional trajectory onto the (ϕ_1, ϕ_2) plane. The additional degrees of freedom could represent the two synaptic gating variables $s_{1,2}(t)$ that evolve according to Eq. (3) (*buffer* variables in the terminology of Golubitsky et al. 2006). Thus, we conclude that the presence of synaptic degrees of freedom is crucial for achieving leap-frog firing in a network of phase oscillators. In particular, the non-zero synaptic decay time course is indispensable in order for such networks to exhibit the change in the firing order. In order to verify the phase description in Fig. 6(a), we constructed its implementation involving two S^1 phase oscillators coupled by continuous synaptic gating variables, and observed leap-frog spiking for an appropriately chosen functional form of the interaction term (see Supplementary Material).

Although non-zero synaptic decay time is a crucial condition for leap-frog spiking in a network of phase oscillators, we find that this dynamical state can also be achieved in a purely pulse-coupled network of oscillators that are *not* phase oscillators on the S^1 phase domain. Figure 6(b) illustrates such a possibility, and can be viewed as the formal limit of the dynamics in Fig. 6(a) with respect to shortening the duration of the synaptic current ("straightening out" the trajectory), while keeping fixed the total amount of phase resetting due to each spike. In this limit the synaptic interaction is no longer continuous, but becomes pulsatile (i.e., it can be described by a delta function). Although the descriptions in panels (a) and (b) are formally similar in terms of the spike sequence and the spike-time phase-resetting values, note that the latter description requires the extension of the phase domain to negative values, and therefore is not a true phase-reduced model. The negative phase value is induced when the spike-triggered phase delay is greater than the inter-spike phase difference between the two cells, i.e. $\Delta(\phi) > \phi$, where $\Delta(\phi)$ is the spike-time response curve (STRC) (described below). Thus, the alternating-order firing state can be obtained in the framework of an extended phase model with instantaneous coupling, with no additional synaptic degrees of freedom, if the phase domain is supplanted with a negative value branch. In particular, in Section 3.7 we show that it can be obtained in a pulse-coupled network of quadratic integrate-and-fire cells. Alternatively, the dynamics in Fig. 6(b) can be implemented by explicitly prohibiting the model cell to spike again if its winding number is not increased since the preceding spike (Brown et al. 2004; Golubitsky et al. 2006). Note however that in the latter case it would be impossible to independently define

the magnitude of phase resetting caused by a second synaptic input that arrives while the postsynaptic cell is still in the negative-phase suppressed subthreshold state.

In the Morris–Lecar model network we consider, the synaptic decay time is short relative to the unperturbed limit cycle period, and the leap-frog spiking corresponds to the phase diagram of Fig. 6(b) rather than Fig. 6(a). In fact, the negative phase has a definite biophysical meaning in this case, and represents the transient suppression of a cell into the subthreshold branch of the trajectory (off the limit cycle) by the inhibitory input, as shown in Figs. 4(b) and 5, allowing the presynaptic cell to pass ahead, reversing the spiking order of the two cells.

3.4 Analysis of existence and stability of periodic alternating-order firing

Although Figs. 5–6 explain qualitatively the dynamics of the alternating-order firing state, we turn to the phase return map approach to study it on a quantitative level. The return map analysis is a powerful method of describing the dynamics of a coupled network (Winfree 2001), but relies on several crucial assumptions. It requires that the cell's spike width and amplitude are invariant and are not affected by the afferent synaptic currents, and also assumes that the perturbation only affects the time to the next spike of the perturbed cell, and has no effect on the dynamics of the cell thereafter. However, this method can be extended to the case where perturbation affects several periods of the post-synaptic cell, under an additional assumption of linear summation of the phase resetting effects due to multiple presynaptic inputs. In fact, Maran and Canavier (2008) demonstrated alternating-order firing in an inhibitory network of type I Wang-Buzsáki model cells in the presence of significant second order phase resetting, although they also showed that alternation in the firing order could emerge in a pulse-coupled map without second-order resetting. We follow the approach of Maran and Canavier (2008), but restrict ourselves to the special case of identical cells, with only first-order phase resetting.

The alternating-order firing is completely characterized by the inter-spike phase sequence labeled $\{\phi_1, \phi_2\}$ in Fig. 7. Here we will construct the return map relating these alternating phase differences, using the phase-resetting curve, or the STRC of each cell, $\Delta(\phi)$. We define $\Delta(\phi)$ to be positive if it produces a phase delay, and negative if it produces a phase advance, with $\phi = 0$ point defined as the peak of the membrane potential, V. $\Delta(\phi)$ is computed numerically, by

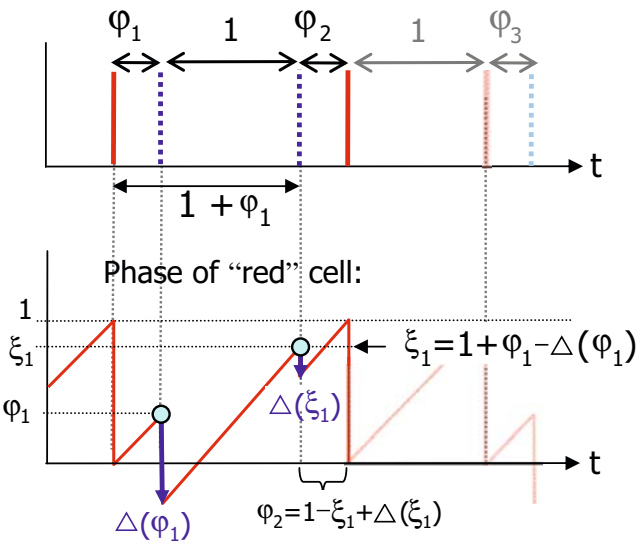

Fig. 7 Constructing the inter-spike phase return map for the periodic alternating-order spiking, $\phi_2 = \Phi(\phi_1)$. In one cycle of the alternating-order spiking, one of the cells spikes twice between two spikes of the partner cell (*dashed blue* and *solid red bars* in *top panel*). The phase intervals ϕ_i are inter-spike intervals normalized by the unperturbed period of each oscillator. *Bottom panel* shows the phase time-course of the cell emitting the *red spikes* in *top panel*. Note that the phase difference between two *dashed blue spikes* equals 1 (the unperturbed period). The phase delays due to each of the two spikes (*blue arrows*) equal $\Delta(\phi_1)$ and $\Delta(\xi_1)$, where ξ_1 is the phase of the cell at the time of arrival of the second input, $\xi_1 = 1 + \phi_1 - \Delta(\phi_1)$. The second inter-spike interval ϕ_2 is found by the first-passage time condition $\xi_1 - \Delta(\xi_1) + \phi_2 = 1$, yielding the phase return map, Eq. (5)

calculating the time between successive membrane potential maxima, while synaptic conductance pulses are applied at different positions of the model cell along the numerically reconstructed limit cycle. The applied perturbation represents a single spike of the presynaptic cell, and is defined numerically by recording the spike-triggered synaptic conductance, $s(t)$ in Eq. (3). Figure 8(a) presents the STRCs for three different values of the synaptic conductance parameter, g_{syn}, corresponding to the distinct activity states shown in panels (a)–(c) of Fig. 1.

The phase return map derived here is a special case of a more general return map derived by Maran and Canavier (2008). Apart from simplifying the analysis, restricting ourselves to the case of a *homogeneous* network with only first-order phase resetting allows us to probe the most elementary conditions on the phase resetting properties required for the change in firing order. Our derivation can be viewed as complementary to the analysis of the order-preserving phase transition map by Goel and Ermentrout (2002), since we explicitly break the map invertibility assumption adopted in that

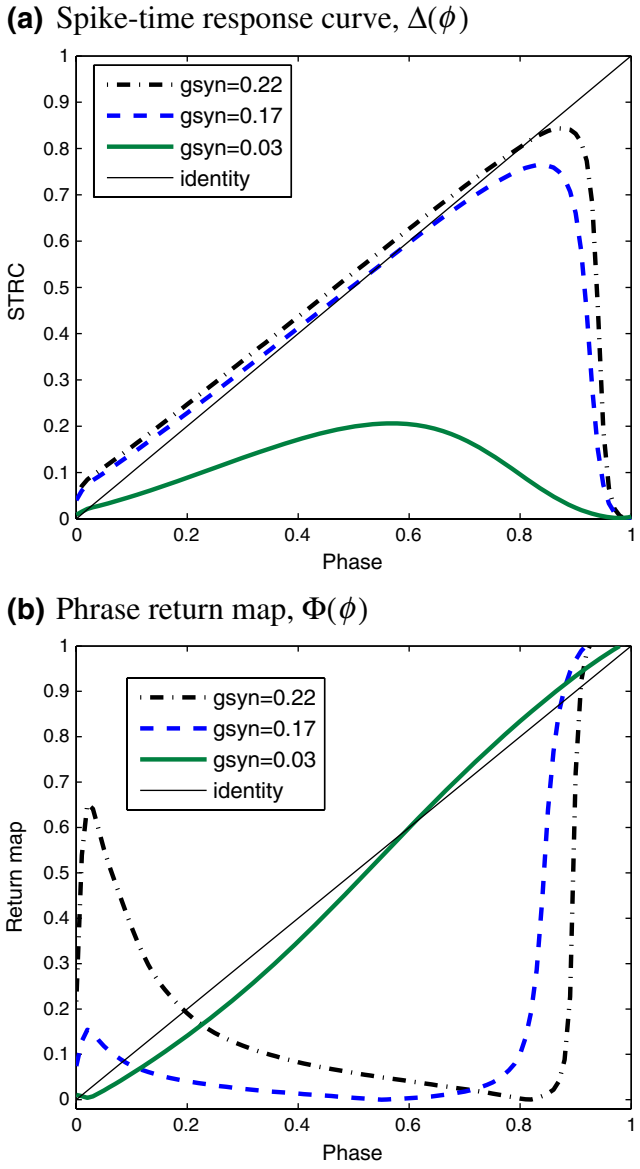

Fig. 8 Phase resetting properties of the Morris–Lecar oscillator. (**a**) Numerically reconstructed STRC, $\Delta(\phi)$, for three different values of coupling strength corresponding to distinct activity patterns (a)–(c) of Fig. 1. (**b**) Phase return maps for each of the three STRCs in panel (**a**); the intersections of each *curve* with the *diagonal line* represent fixed points of that map. For $g_{syn} = 0.03$, the order-preserving map is shown, with only one stable fixed point at $\phi = 0^+$ ($\phi = 1^-$), corresponding to synchronous firing. The two curves corresponding to $g_{syn} = 0.17$ and $g_{syn} = 0.22$ show both the order-alternating phase map (Eq. (5)) on the phase interval where $\Delta(\phi) > \phi$, and the order-preserving map of Goel and Ermentrout (2002) on the portion of the phase domain where $\Delta(\phi) < \phi$. Note that there is one stable fixed point for $g_{syn} = 0.17$ corresponding to leap-frog spiking, while the alternating order fixed point for $g_{syn} = 0.22$ is unstable, leading to period-2 leap-frog dynamics shown in Fig. 1(c). The order-preserving fixed point on the right end of the interval is unstable for both $g_{syn} = 0.17$ and $g_{syn} = 0.22$

study (condition 2 on p. 199 therein), by allowing the phase variable to turn negative. The case of strong phase resetting was previously considered in the analysis of strongly coupled neurons by Acker et al. (2003) (see also Jones et al. 2000; Kopell et al. 2000, and Netoff et al. 2005), and in the study of strongly forced oscillators by Glass et al. (1984).

Note that the homogeneous network case implies a permutation symmetry between the two neurons, which means that the map relating phases ϕ_2 and ϕ_1 in Fig. 7 is identical to the map relating phases ϕ_3 and ϕ_2. Therefore, it is sufficient to analyze the phase dynamics of only one of the two cells, while it receives two spikes from its partner cell. Let ϕ_1 denote the phase of cell 1 (*red* spike and *red* trace in Fig. 7) at the arrival time of the first synaptic current pulse due to the spike of the pre-synaptic cell (dashed blue line), where phase is defined as the time since the last spike, normalized to unperturbed oscillation period. The amount of phase delay induced by the synaptic input at phase ϕ_1 equals $\Delta(\phi_1)$, since we define phase delay as positive phase resetting, contrary to the sign convention of Goel and Ermentrout (2002). For sufficiently strong synaptic inhibition this phase reset satisfies $\Delta(\phi_1) > \phi_1$ which delays the first passage time to next spike of the post-synaptic cell (cell 1) to a value greater than 1, the intrinsic (uncoupled) oscillation period. Note that this breaks the conditions on the STRC assumed by Goel and Ermentrout (2002). As a result, the pre-synaptic cell 2 has a chance to spike again (second dashed line), after a phase interval corresponding to the unperturbed oscillation period, $\Delta\phi = 1$, since cell 2 receives no input from cell 1 during this period. This second synaptic current from cell 2 arrives when the phase of cell 1 equals $\xi_1 \equiv 1 + \phi_1 - \Delta(\phi_1)$, which takes into account the delay due to the first spike. Therefore, the second spike induces a phase delay equal to $\Delta(1 + \phi_1 - \Delta(\phi_1))$. It is only after receiving this second input that cell 1 finally has a chance to spike, after a phase interval defined as ϕ_2. The total phase delay due to both inputs is thus equal to

$$\phi_1 + \phi_2 = \Delta(\phi_1) + \Delta(1 + \phi_1 - \Delta(\phi_1))$$

Therefore, the return map for the phase intervals ϕ_i is given by

$$\phi_2 \equiv \Phi(\phi_1) = \Delta(\phi_1) + \Delta(1 + \phi_1 - \Delta(\phi_1)) - \phi_1 \qquad (5)$$

or, expressed in terms of the phase of the post-synaptic cell at the time of arrival of the second spike, $\xi_1 = 1 + \phi_1 - \Delta(\phi_1)$:

$$\phi_2 \equiv \Phi(\phi_1) = 1 + \Delta(\xi_1) - \xi_1 \tag{6}$$

Figure 8(b) shows this phase transition map for each of the three STRCs shown in panel (a). Note that this map is only defined on the phase domain where $\Delta(\phi) > \phi$. On the rest of the domain, Fig. 8(b) shows also the order-preserving map of Goel and Ermentrout (2002). Fixed points of map (5)–(6) correspond to the periodic 2:2 alternating-order (leap-frog) activity:

$$\phi = 1 + \Delta(\xi) - \xi \tag{7}$$

Since $\xi \equiv 1 + \phi - \Delta(\phi)$, this condition can be written in a more symmetric form

$$\phi = \frac{\Delta(\phi) + \Delta(\xi)}{2} \tag{8}$$

Taking into account the constraint on the phase domains, $\xi \leq 1$ and $\Phi(\phi) \leq 1$, we also obtain

$$\Delta(\phi) > \phi \tag{9}$$

$$\Delta(\xi) < \xi \tag{10}$$

Conditions (8–10) are examined geometrically in Fig. 9. Note that the synchronous firing solution $\{\phi = 0^+, \xi = 1^-\}$ always satisfies the periodicity condition (8), if one assumes $\Delta(0^+) = \Delta(1^-) = 0$.

If the inequality $\xi \leq 1$ is violated (i.e. when $\Delta(\phi) < \phi$), the cells fire sequentially, so their firing order does not alternate, while the violation of the condition $\Phi(\phi) \leq 1$ (i.e. if $\Delta(\xi) > \xi$) indicates that the postsynaptic cell will emit more than two consecutive spikes. The latter is true for instance for n:n bursting states with $n > 2$ (see Fig. 1(d)), in which case one can derive an extended map analogous to Eq. (5). An additional alternating-order constraint $\Phi(\phi) > 0$ requires that $\Delta(\xi) > -(1 - \xi)$. This condition is automatically satisfied if the resetting is sign-definite (pure delay resetting).

Stability of the 2:2 periodic spiking depends on the value of the derivative of the phase map given by Eq. (5) at equilibrium:

$$\Phi'(\phi) = [\Delta'(\xi) - 1][1 - \Delta'(\phi)] \tag{11}$$

The fixed point will be stable if $|\Phi'(\phi)| < 1$. Therefore, the periodic alternating-order firing is stable when the slope of the STRC at the time of arrival of either of the two synaptic inputs (corresponding to phases ϕ and $\xi = 1 + \phi - \Delta(\phi)$) is sufficiently close to 1. This is equivalent to the stability condition derived by Maran and Canavier (2008). The stability of synchronous firing is determined by an analogous map slope expression, with $\phi = 0^+$ and $\xi = 1^-$ (Eq. 12 in Goel and Ermentrout 2002). Since $\Delta'(1) \approx 0$ in the Morris–Lecar model (see Fig. 10), the bifurcation from synchronous to leap-frog firing occurs when the slope $\Delta'(\phi)$ at $\phi = 0$ becomes greater than 2, forcing ϕ to increase (and thus ξ to decrease) until the stability condition is satisfied. Thus, the characteristic sharp initial rise of $\Delta(\phi)$ followed by a less steep increase at larger ϕ, seen both in Figs. 8(a), 9 of this work, and in Fig. 2(b) of Maran and Canavier (2008), is essential for the transition from synchronous to leap-frog spiking. This feature corresponds to the characteristic dip to negative values in the phase transition return map noted by Maran and Canavier (2008).

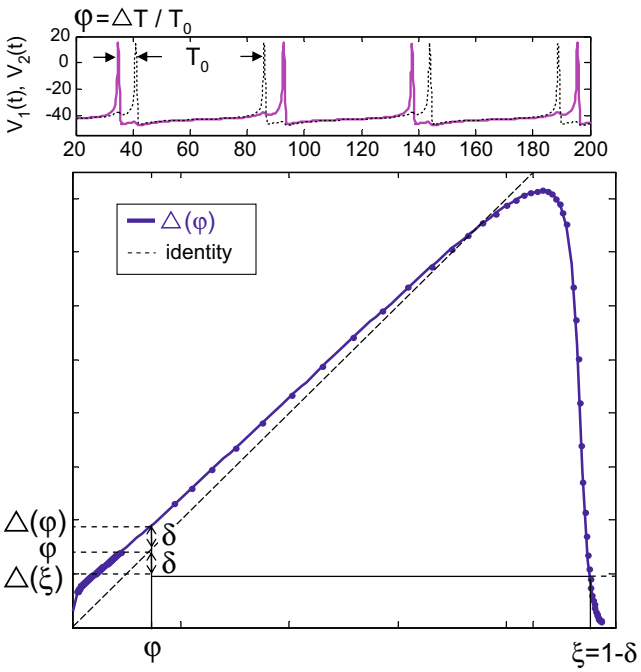

Fig. 9 Phase-map analysis of alternating-order spiking. *Top panel* shows the cell potential time course of the two coupled ML oscillators as *red* and *black traces*, for $\bar{g}_{syn} = 0.2$. Equilibrium inter-spike phase difference ($\phi = 0.144$) in the alternating-order state satisfies Eq. (7). Note that $\delta = \Delta(\phi) - \phi = \phi - \Delta(\xi)$, where ξ is the phase of the postsynaptic cell at the time of arrival of the second spike, $\xi = 1 - \delta$. In this simulation, $\delta = 0.0468$, and $\Delta(1 - \delta) = 0.095$. The stability condition given by Eq. (11) is satisfied

Finally, let's briefly consider the case where the intervals ϕ_1 and ϕ_2 between the spikes of the pre- and

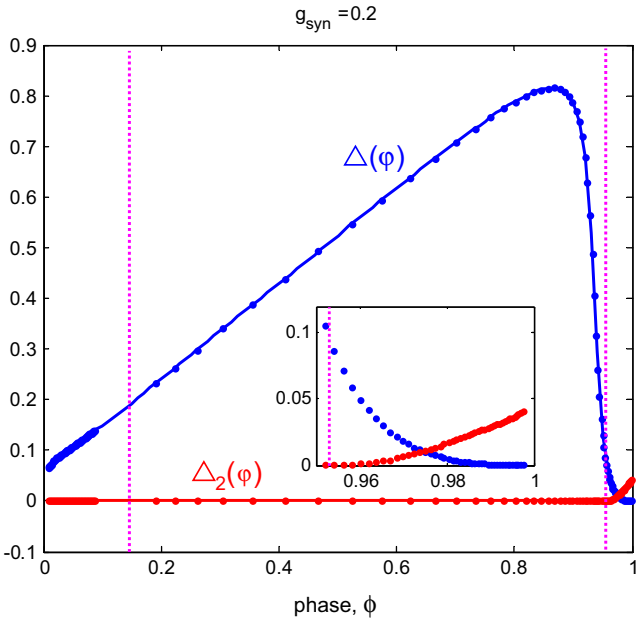

Fig. 10 Comparison between the first- and the second-order STRCs of the Morris–Lecar oscillator. The first-order STRC is shown in *blue* ($\Delta(\phi)$), while the second-order STRC is shown in *red* ($\Delta_2(\phi)$), for synaptic conductance of $\bar{g}_{syn} = 0.2$. The *inset* zooms in on the part of the phase domain where $\Delta_2(\phi)$ is non-negligible. The two functions satisfy the consistency condition $\Delta(0^+) = \Delta_2(1^-)$. *Vertical dashed lines* mark the two phase intervals characterizing the leap-frog state, ϕ and ξ in Fig. 9. Note that $\Delta_2(\phi) = 0$, $\Delta_2(\xi) \simeq 1.4 \cdot 10^{-4}$, therefore second-order phase resetting does not contribute to the alternating-order dynamics for this value of coupling strength

the post-synaptic cells alternate between two distinct values, as in Fig.1(c). We call this state the period-2 alternating-order 2:2 firing, since it results from the period-doubling of the equal-phase alternating-order state (Fig. 2). Both ϕ_1 and ϕ_2 are period-2 fixed points of the map given by Eq. (7), i.e. $\Phi(\Phi(\phi_{1,2})) = \Phi(\phi_{2,1}) = \phi_{1,2}$, therefore

$$\Phi(\phi_1) = 1 + \Delta(\xi_1) - \xi_1 = \phi_2$$
$$\Phi(\phi_2) = 1 + \Delta(\xi_2) - \xi_2 = \phi_1 \qquad (12)$$

where $\xi_i = 1 + \phi_i - \Delta(\phi_i)$, $i = 1, 2$. We note that our choice of the "period-2" designation is somewhat arbitrary, since it can also be applied to the equal-phase leap-frog spiking: both of these states are characterized by a period-2 trajectory of each cell in its phase space, composed of two unequal loops comprising one period of the oscillation (see Fig. 5). Note also that the cell permutation symmetry does not hold in this case, and therefore this map is closer to the more general leap-frog spiking map derived by Maran and Canavier (2008). The stability of period-2 leap-frog spiking depends on the derivative of the map $F(\phi) = \Phi(\Phi(\phi))$ at equilibrium values ϕ_1 and ϕ_2: $\Phi'(\phi_2)\Phi'(\phi_1) = [\Delta'(\xi_1) - 1][1 - \Delta'(\phi_1)][\Delta'(\xi_2) - 1][1 - \Delta'(\phi_2)]$. We note that this stability conditions is equivalent to the stability condition for a sequential phase-locked mode obtained by Oprisan and Canavier (2001) (see also Oprisan et al. 2004).

An important feature of higher-period 2:2 modes is the large value of the equilibrium inter-spike interval relative to the unperturbed period. In the ML network we consider, this interval can constitute as much as 70% of the uncoupled oscillation period (Figs. 1(c), 2), and is an order of magnitude larger than the time scale of synaptic interaction that underlie this dynamic state.

3.5 Second-order STRC

Figure 10 shows that the second-order phase resetting $\Delta_2(\phi)$ is non-zero only for phase values close to 1, since the synaptic time constant is short ($\tau_{syn} = 1-2$ ms). For the two characteristic phases in Fig. 9, the second-order phase resetting values equal $\Delta_2(0.144) \approx 0$ and $\Delta_2(0.9532) \approx 1.4 \cdot 10^{-4}$. Therefore, second-order resetting provides only negligible contribution to the alternating-order periodic firing shown in top panel of Fig. 9. This is to be contrasted with the network of Wang-Buzsáki model cells studied by Maran and Canavier (2008), who showed that 2-nd order phase resetting provides a more significant, albeit not necessary, contribution to leap-frog spiking in that network.

Although the second-order phase resetting is not critical to achieving stable alternating-order activity, it will influence the critical value of $\bar{g}_{syn}$ at the bifurcation from synchrony to leap-frog spiking, since it affects the stability of both states. Noting once again that the second-order phase-resetting is negligible for small values of the phase, we find that the map slope previously given by Eq. (11) is modified according to (see Appendix for derivation):

$$\Phi'(\phi) = [\Delta'(\xi) - 1][1 - \Delta'(\phi)] + \Delta_2'(\xi) \qquad (13)$$

In particular, synchronous firing is stable if

$$|[\Delta'(1^-) - 1][1 - \Delta'(0^+)] + \Delta_2'(1^-)| < 1 \qquad (14)$$

Further, taking into account the small slope of the first-order STRC at $\phi = 1$ (see Fig. 10), we obtain an approximate condition

$$|\Delta'(0^+) + \Delta_2'(1^-) - 1| < 1$$

Since both derivatives are positive, synchrony is stable if

$$\Delta'(0^+) + \Delta_2'(1^-) < 2 \qquad (15)$$

Therefore, the bifurcation from synchronous to leap-frog spiking occurs when $\Delta'(0^+) + \Delta_2'(1^-) = 2$. The stability condition (Eq. (13)) suggests that second-order phase resetting has a generally destabilizing effect on both synchronous and alternating-order activity. This agrees with our finding that stable alternating-order spiking cannot be achieved when τ_{syn} is comparable to the length of the uncoupled oscillation period (see Section 3.8).

3.6 Effect of variation in coupling strength

Given the knowledge of the STRC, one can readily determine the stable network activity modes for the corresponding value of the coupling strength. However, the full range of activity states demonstrated in the bifurcation diagram of Fig. 2 requires one to know the STRC at each value of the synaptic conductance. In the case of weak coupling, the STRC is assumed to scale linearly with the strength of the coupling, a condition which is violated in the case of non-weak interactions that we consider, as shown in Fig. 8(a). In particular, the right-ward shift in the peak of the STRC curve evident in Fig. 8(a) is a well-known feature of the Morris–Lecar model (Ermentrout 1996). The question then arises whether this change in the shape of the STRC has a qualitative effect on the bifurcation structure of the network dynamics shown in Fig. 2, or whether this bifurcation structure describes a stereotypical period doubling cascade, representing universal behavior expected for a large class of STRC functions with respect to a simple scaling of their amplitudes.

To verify the generality of the observed leap-frog spiking and the associated bifurcation structure, we considered the case of a quadratic STRC defined as $\Delta(\phi) = 4m\phi(1-\phi)$. Note that the STRC of this shape agrees with the existence conditions for leap-frog spiking, illustrated in Fig. 9, as does any continuous function with a sharp initial rise and downward concavity at small phases, and decaying to zero as the phase approaches 1^-. We employed the "emulator" algorithm introduced by Canavier et al. (1999) to artificially generate the "inter-spike" phase sequence for the quadratic STRC, and explored the effect of increasing the STRC amplitude, m. We verified that the entire bifurcation structure of the ML network dynamics is reproduced by the quadratic STRC emulator, and is presented in Fig. 11 (cf. Fig. 2). Note that the map amplitude corresponding to the bifurcation from synchronous to alternating-order firing can be obtained analytically for the case of quadratic PRC, using Eq. (11): $\Phi'(0) > 1$ for $m > m_{crit} = 2^{-3/2}$ (see Fig. 11). The bifurcation to the oscillator death is also easily analyzed,

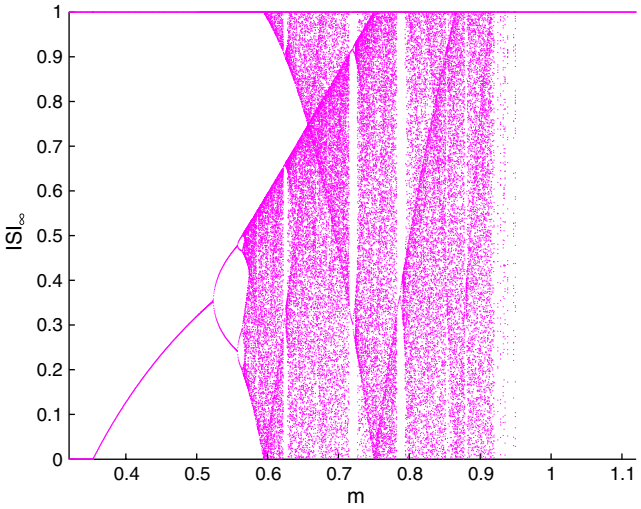

Fig. 11 Emulated bifurcation diagram for the inter-spike (inter-event) interval differences as a function of the amplitude of a quadratic STRC, $\Delta(\phi) = 4m\phi(1-\phi)$. Asymptotic inter-spike interval differences ISI_∞ are plotted as a function of the STRC peak amplitude, m. Bifurcation from synchronous to alternating-order event sequence occurs at $m_{crit} = 2^{-3/2}$, while the oscillator death requires $m \geq 1$. Note that bursting dynamics similar to Fig.1(e) is also obtained, for instance for $m = 0.785$

and occurs at $m = 1$. Finally, the bursting states such as the one shown in Fig. 1(e) are also obtained using the quadratic STRC. Although it is well-known that the iteration of a quadratic map leads to a period-doubling cascade and chaos, these results are of value in proving that the alternating-order firing is a general phenomenon for models characterized by STRC of a given shape, and that the observed bifurcation structure is explained by the change in STRC amplitude only, and does not require a change in the shape of the STRC characteristic of the Morris–Lecar oscillator.

3.7 Alternating-order spiking in a pulse-coupled network

As discussed in Section 3.3, leap-frog spiking can be achieved in a purely pulse-coupled network if the coupled cells do not represent phase oscillators, but include an additional subthreshold branch, implemented for instance by augmenting the standard S^1 phase domain with a negative phase value interval, leading to the dynamics in Fig. 6(b). This negative-phase branch represents the tail of the "tadpole"-shaped trajectory shown in Fig. 5(b). The topology of such an extended phase model is in fact equivalent to the topology of an integrate-and-fire class of models, as noted by Golubitsky et al. (2006). If a given IF model includes a finite reset potential, then the interval between such

reset value and the threshold potential can be identified with an S^1 phase domain. However, an inhibitory perturbation of sufficient strength can lower the voltage of a cell below the reset value, which can be viewed as a negative phase.

Since the standard integrate-and-fire model is characterized by a monotonically increasing STRC with downward concavity (Mirollo and Strogatz 1990), it does not satisfy leap-frog firing existence conditions, Eqs. (8–10). However, the *quadratic* integrate-and-fire model (QIF) is a more promising candidate, due to its close association with the canonical model of type-I SNIC excitability bifurcation (Ermentrout 1990, 1996; Hoppensteadt and Izhikevich 1997). In order to satisfy the leap-frog existence conditions, we modify the standard non-dimensionalized QIF model, $dv/dt = v^2 + 1$, by assuming finite threshold and reset values, which we set asymmetrically to $v_t = 5$ and $v_r = -1$, respectively, in order to obtain an STRC shown in Fig. 12(a). This STRC shares the characteristic shape of the STRC of the Morris–Lecar model shown in Figs. 8 and 9, and therefore it too satisfies the leap-frog spiking conditions, Eqs. (8–10). Figure 12(b) shows the corresponding phase return map for the three different values of pulse amplitude, illustrating both the order alternating and the order preserving maps. For each of the three chosen values of the coupling strength, the order-alternating state is stable. Although a finite threshold value is not necessary for achieving alternating-order firing, note that a finite reset value is crucial for creating a multi-branched phase domain.

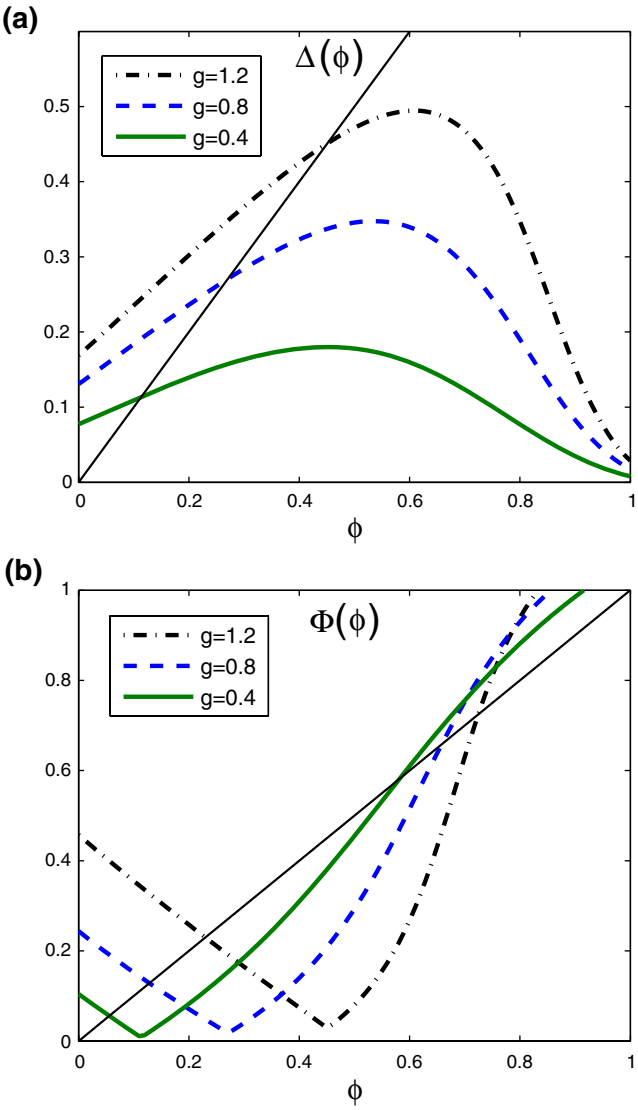

Fig. 12 Phase-resetting analysis of a pulse-coupled network of two quadratic integrate-and-fire cells, $dv_i/dt = v_i^2 + 1 - g\ \delta(t - t_j)$, with asymmetric threshold and reset values, $v_t = 5$ and $v_r = -1$ (**a**) STRCs for pulse amplitude values of $g = 0.4$, 0.8, and 1.2 are given by $\Delta(\phi) = \phi + [\arctan v_r - \arctan(\tan(T\phi + \arctan v_r) - g)]/T$, where $T = \arctan v_t - \arctan v_r$ is the oscillation period. (**b**) Phase return maps corresponding to each of the STRCs shown in (**a**). As in Fig. 8, each of the three curves switches from order-alternating to order-preserving map at point $\phi = \Delta(\phi) = [\pi/4 + \arctan(g - 1)]/T$. For each value of g, there is one stable leap-frog spiking fixed point, and one unstable fixed point corresponding to phase-locked order-preserving dynamics. The equal-phase (period-1) leap-frog spiking is stable for $g < 4/3$

3.8 Effect of increasing synaptic decay time

The dynamics of the two-cell network that we study undergoes a qualitative change as the synaptic decay time is increased beyond short durations of 1–4 ms. Namely, we observe emergence of bistability between synchronous spiking and alternating-order dynamics, and a narrower domain of stability of the alternating-order state, which disappears completely when the synaptic decay time becomes longer than about 1/6 of the unperturbed oscillations period in our ML model. Note that bistability between synchrony and leap-frog spiking was also observed by Maran and Canavier (2008) in the Wang-Buzsáki model network. This change in dynamics can be understood in terms of the measured changes in the first- and second-order STRC, shown in Fig. 13. The two panels (a) and (b) of this Figure also present the phase return map, $\Phi(\phi)$, for synaptic decay times of 6 and 7 ms, respectively. Note that the second-order STRC becomes more pronounced at larger τ_{syn}, which is associated also with an increase in non-zero value of the 1-st order STRC at zero phase. Therefore, the second-order STRC cannot be ignored, leading to the modified stability conditions, Eq. (13), derived in the Appendix (Eq. (21)) and approximated as $\Delta'(\phi) + \Delta_2'(\xi) < 2$ (Eq. (22)). Note that the increase in $\Delta(0^+)$ is associated with a decrease in the initial

slope of the STRC at longer synaptic decay time, as is evident in Fig. 13 (cf. Fig. 8). This leads to stable synchronous firing, achieved when $0 < \Delta'(0^+) + \Delta_2'(1^-) < 2$ (Eq. (15)), and results in the bistability between synchronous and leap-frog spiking, captured by the alternating-order phase return maps shown in Fig. 13.

Finally, we note that the STRC analysis is not applicable if the synaptic decay time is large enough to be comparable in duration to the interval between incoming spikes.

3.9 Three-cell network

In order to explore the effects of non-weak inhibitory coupling in a larger network, we simulated the dynamics of three identical neuron with all-to-all coupling, and observed a diversity of network behaviors that are analogous to the activity states exhibited by a two-cell network. As the coupling strength ($\bar{g}_{syn}$) is increased, the synchronized state becomes unstable, giving way to the alternating order state shown in Fig. 14, which is followed by a period-doubling cascade to chaotic activity, and at sufficiently strong value of the coupling we observe the transition to the oscillator death mode. Note that in the three-neuron network, the alternating order state represents a splay state (Fig. 14). Our results are in agreement with the results of Maran and Canavier (2008) for the heterogeneous network of Wang-Buzsáki model neurons. Larger networks of up to ten neurons were examined by Maran and Canavier (2008), who described similar activity states, with an additional property of clustering, whereby distinct synchronized subgroups of neurons fire in a splay-state temporal order (see Fig. 12 therein).

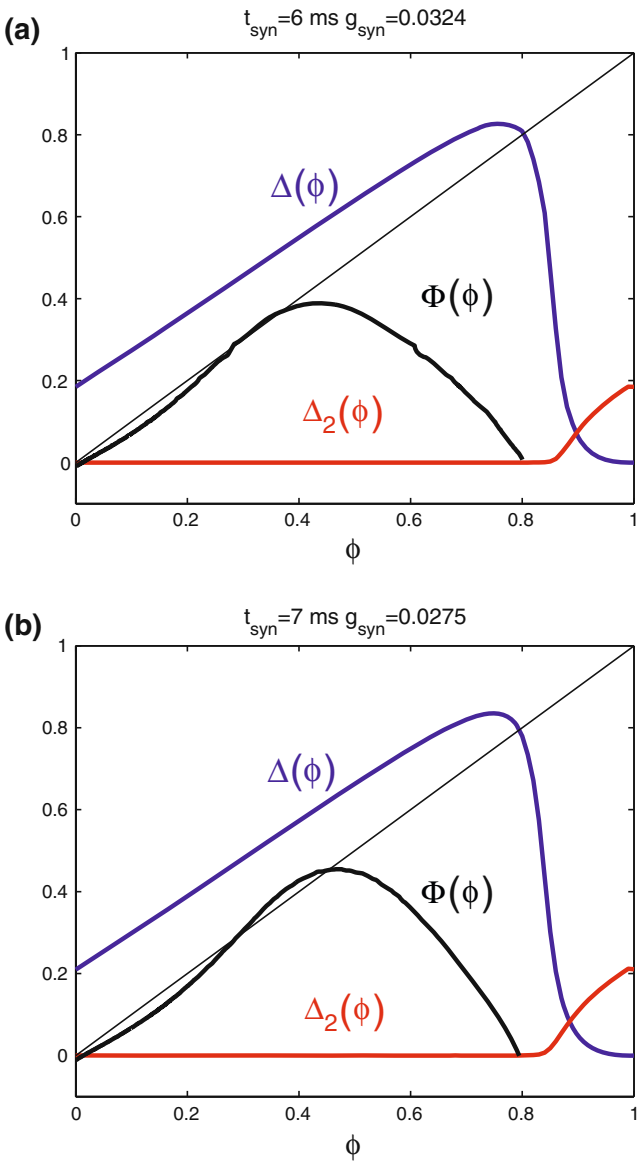

Fig. 13 Longer synaptic decay leads to bistability between synchronous and leap-frog dynamics. Each of the two panels shows the first-order STRC ($\Delta(\phi)$, *blue*), second-order STRC ($\Delta_2(\phi)$, *red*) and the phase-return map (*black*) for $\tau_{syn} = 6$ ms in (**a**) and $\tau_{syn} = 7$ ms in (**b**). Note the two stable and one unstable fixed points for each τ_{syn}, with one stable equilibrium at the origin, corresponding to synchronous firing, and another stable fixed point corresponding to leap-frog spiking

4 Discussion

We have shown that the non order-preserving activity recently observed by Maran and Canavier (2008) in an inhibitory network of Wang-Buzsáki oscillators can also be obtained in a network of lower-dimensional Morris–Lecar model neurons, and therefore is a general property of a wider class of type-I excitable cells. Namely, we found that such "leap-frog" dynamics results when the inhibition from one cell is sufficient to transiently bring the post-synaptic cell below the excitability threshold, producing a phase delay that is greater than the time elapsed since the preceding spike. This further illustrates the fact that the range of applicability of the weak coupling results is quite narrow in inhibitory networks of type I cells that are close to their excitation thresholds (Hoppensteadt and Izhikevich 1997. As the coupling strength is increased, the leap-frog spiking state gives way to a period-doubling cascade, leading to more complex *m*:*n* periodic bursting states, as well as chaotic activity. Finally, at sufficiently strong values of the coupling strength oscillator death occurs, whereby only one of the cells continues spiking, suppressing the activity of the post-synaptic cell.

One of our goals was to reveal the conditions required for alternating-order dynamics, and we showed

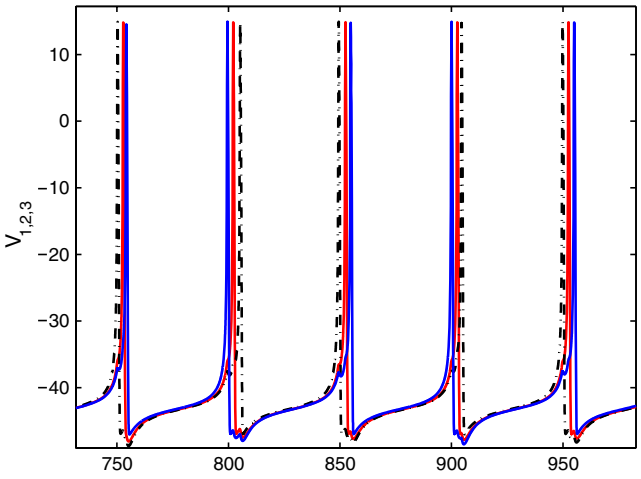

Fig. 14 Network of three all-to-all coupled ML oscillators exhibits splay states in a certain range of synaptic coupling strength ($\bar{g}_{syn} = 0.14$). The potentials of the three cells are shown as *black*, *red*, and *blue* traces. Note the change in spiking order: 1,2,3 → 3,2,1 → 1,2,3 → ...

that it can be achieved under two different sets of conditions. First, it can be exhibited by a network of phase oscillators, in the presence of independent synaptic degrees of freedom with non-zero synaptic decay time. Second, leap-frog spiking is also possible in networks of oscillators whose dynamics cannot be reduced to a single phase variable. In this case order alternation can be achieved even in a purely pulse-coupled network. This is true in particular for a network of appropriately modified quadratic integrate-and-fire model cells (Fig. 12). The ML network we examined also falls within the latter class of models, in that order alternation is achieved for very short synaptic decay time, and the periodic trajectory of each cell significantly deviates from the unperturbed limit cycle due to periodically received inhibition.

In both classes of models, order alternation implies the same conditions on the phase resetting characteristic of the coupled cells. To establish these conditions, we followed the approach of Maran and Canavier (2008), but restricted ourselves to the case of a homogeneous network, in order to determine the most basic requirements leading to spiking order alternation (Eqs. (8–10)). The principle condition for order alternation is that the phase delay produced by an input arriving shortly after the spike-time should be larger than the time elapsed since this last spike, $\Delta(\phi) > \phi$. Thus, the phase-transition map (Eq. (5)) is complementary to the map of Goel and Ermentrout (2002) derived under the assumption of phase map invertibility, $\Delta(\phi) < \phi$. In a pulse-coupled network, such strong resetting automatically breaks the phase structure of each oscillator, since it leads to a delay past the spike-time, requiring an additional negative-phase domain branch, or, alternatively, an additional condition that a cell does not emit a spike unless its winding number is increased (Brown et al. 2004; Golubitsky et al. 2006). In contrast, in a network of cells with a non-zero synaptic decay time this complication does not arise, since such strong phase delay resetting is spread out over a finite time interval, and the phase variable may remain positive. For the Morris–Lecar model in the type-I parameter regime we consider, this strong phase resetting property is directly related to the fast kinetics of the K^+ channels relative to the rate of change of the membrane potential, which clamps the trajectory to the w-nullcline during the quiescent subthreshold phase of the limit cycle. An inhibitory current pulse applied in this oscillation phase perturbs the dynamics along the w-nullcline, which plays the role of a slow manifold, allowing to achieve a phase delay greater than the time to the preceding spike.

Finally, we showed that the entire bifurcation structure of the network, involving a period-doubling cascade to chaos, and more complex $m : n$ mode-locked bursting patterns, can be explained by a simple scaling of the STRC amplitude, and therefore does not require a non-trivial change in the shape of the STRC arising from the biophysics of a particular cell model. Note that there are other STRC shapes consistent with leap-frog spiking. Full analysis of STRC functions supporting leap-frog spiking is beyond the scope of the current work.

Our results for the Morris–Lecar network hold in a certain range of synaptic decay times that are significantly shorter than the uncoupled period of each cell. In the particular parameter regime we consider, second-order phase resetting effects become significant and can no longer be ignored when the synaptic decay time becomes larger than about 1/8 of the unperturbed oscillation period. In this case we see significant bistability between the synchronous and alternating-order states (Fig. 13), which is consistent with the observed change in the shape of the STRC with increasing τ_{syn}. As the synaptic decay time is increased, the region of attraction of the leap-frog state shrinks, and at sufficiently large τ_{syn}, the homogeneous network is no longer capable of sustaining leap-frog activity. In this case significant heterogeneity may be required to destabilize phase-locking; this conjecture is in agreement with the results of Maran and Canavier (2008).

These results and the results of Maran and Canavier (2008) further illustrate the qualitative features of periodic spike train patterns that can be produced by simple inhibitory networks of cells with type-I excitability,

beyond the simple phase-locked firing states that can be predicted using the weak-coupling theory (see also White et al. 1998). This may have implications for the study of central pattern generators, which are responsible for producing distinct firing sequences, for instance in enervating opposing muscle groups during motor activity, and which often contain subnetworks of several cells coupled by reciprocal inhibition. We note that the classification of possible network activity states, and its relationship to the underlying network architecture and the qualitative properties of cell dynamics, is a subject of significant recent interest (Golubitsky et al. 1999, 2006; Acker et al. 2003).

Finally, it would be interesting to explore whether the phenomenon we describe is even more general, and whether similar dynamical behavior is exhibited by non-weakly coupled cells of a different excitability class, satisfying the crucial condition of strong phase delay, $\Delta(\phi) > \phi$. Note that the phase-resetting characteristic of oscillators outside of the type-I excitability class can change the sign over part of its phase domain (Ermentrout 1996). If an inhibitory synaptic input produces a phase advance rather than a phase delay, then order alternation may in principle be achieved in an *excitatory* network of such cells, given that the conditions (8-12) on their phase resetting properties are satisfied.

Acknowledgements This work was supported by the National Science Foundation grant DMS-0417416. We wish to thank Amitabha Bose and Farzan Nadim for helpful comments and discussions.

Appendix

Derivation of the alternating-order phase map with second-order phase resetting

We will use the diagram in Fig. 7(a) to derive the map in the case of non-negligible second-order phase resetting, $\Delta_2(\phi)$. Let $\{\phi_n, \xi_n\}$ denote the two phases of the postsynaptic cell at the time of arrival of each of the two spikes in n-th period of the oscillation. In the case of zero second-order resetting, Fig. 7 illustrates the relationship between these phases, $\xi_n = 1 + \phi_n - \Delta(\phi_n)$. However, due to non-zero second-order phase resetting received by the presynaptic cell in the preceding cycle, $\Delta_2(\xi_{n-1})$ (where ξ_{n-1} is its phase at the time of arrival of the first black spike in Fig. 7(a)), the interval between two spikes of the presynaptic cell in the current cycle, denoted γ_n, will not be equal to 1:

$$\gamma_n = 1 + \Delta_2(\xi_{n-1}) > 1 \tag{16}$$

Therefore, the modified relationship between ξ_n and ϕ_n reads

$$\xi_n = \gamma_n + \phi_n - \Delta(\phi_n) \tag{17}$$

Note that we neglect the much smaller second-order phase-resetting due to the first spike of the presynaptic cell in each period of the 2:2 mode: $\Delta_2(\phi_n) << \Delta_2(\xi_n)$. Finally, given the phase ξ_n of the postsynaptic cell right before receiving its second input, one can easily find its first passage time, ϕ_{n+1} (i.e. interval ϕ_2 in Fig. 7(a)), using the first passage time condition

$$\xi_n - \Delta(\xi_n) + \phi_{n+1} = 1 \tag{18}$$

Solving this system of equations for ξ_n yields the map

$$\xi_{n+1} = 2 - \xi_n + \Delta(\xi_n) - \Delta(1 - \xi_n + \Delta(\xi_n)) + \Delta_2(\xi_n) \tag{19}$$

which can be re-written in a more compact form as

$$\xi_{n+1} = 1 + \phi_{n+1} - \Delta(\phi_{n+1}) + \Delta_2(\xi_n) \tag{20}$$

If we substitute the conditions for synchronous firing, $\xi_n = 1$, $\phi_n = 0$, we obtain $\Delta_2(1) = \Delta(0)$, which is the correct periodicity condition relating the first- and second-order STRC curves. Therefore, the synchronous solution is always a fixed point of Eq. (19).

Differentiating Eq. (20) yields the stability condition

$$|[1 - \Delta'(\phi)][\Delta'(\xi) - 1] + \Delta_2'(\xi)| < 1 \tag{21}$$

which agrees with Eq. (11) when $\Delta_2(\cdot)$=0. Close to the bifurcation from synchrony to leap-frog spiking, $\xi \approx 1$, $\Delta'(\xi) \approx 0$, and therefore

$$|\Delta'(\phi) + \Delta_2'(\xi) - 1| < 1$$

which yields

$$0 < \Delta'(\phi) + \Delta_2'(\xi) < 2 \tag{22}$$

Recall that $\phi = 1 - \xi + \Delta(\xi)$ (Eq. (18)). A more general stability condition for the case of non-negligible $\Delta_2(\phi_n)$ is given by Maran and Canavier (2008).

References

Acker, C. D., Kopell, N., & White, J. A. (2003). Synchronization of strongly coupled excitatory neurons: Relating network behavior to biophysics. *Journal Comparative Neuroscience, 15*, 71–90.

Bose, A., Kopell, N., & Terman, D. (2000). Almost synchronous solutions for pairs of neurons coupled by excitation. *Physica D, 140*, 69–94.

Bressloff, P. C., & Coombes, S. (1998). Desynchronization, mode locking, and bursting in strongly coupled integrate-and-fire oscillators. *Physical Review Letters, 81*, 2168–2171.

Bressloff, P. C., & Coombes, S. (2000). Dynamics of strongly-coupled spiking neurons. *Neural Computation, 12*, 91–129.

Brown, E., Moehlis, J., & Holmes, P. (2004). On the phase reduction and response dynamics of neural oscillator populations. *Neural Computation, 16*, 673–715.

Canavier, C. C., Baxter, D. A., Clark, J. W., & Byrne, J. H. (1999). Control of multistability in ring circuits of oscillators. *Biological Cybernetics, 80*, 87–102.

Ermentrout, G. B. (1996). Type I membranes, phase resetting curves, and synchrony. *Neural Computation, 8*, 979–1001.

Ermentrout, G. B., & Kopell, N. (1984). Frequency plateaus in a chain of weakly coupled oscillators. *SIAM Journal on Mathematical Analysis, 15*, 215–237.

Ermentrout, G. B., & Kopell, N. (1990). Oscillator death in systems of coupled neural oscillators. *SIAM Journal on Applied Mathematics, 50*, 125–146.

Ermentrout, G. B., & Kopell, N. (1991). Multiple pulse interactions and averaging in systems of coupled neural oscillators. *Journal of Mathematical Biology, 29*, 195–217.

Glass, L., Guevara, M. R., Belair, J., & Shrier, A. (1984). Global bifurcations of a periodically forced biological oscillator. *Physical Review, A 29*, 1348–1357.

Goel, P., & Ermentrout, G. B. (2002). Synchrony, stability, and firing patterns in pulse-coupled oscillators. *Physica D, 163*, 191–216.

Golubitsky, M., Stewart, I., Buono, P. L., & Collins, J. J. (1999). Symmetry in locomotor central pattern generators and animal gaits. *Nature, 401*, 693–695.

Golubitsky, M., Josic, K., & Shea-Brown, E. (2006). Winding numbers and average frequencies in phase oscillator networks. *Journal of Nonlinear Science, 16*, 201–231.

Hansel, D., Mato, G., & Meunier, C. (1995). Synchrony in excitatory neural networks. *Neural Computation, 7*, 307–337.

Hoppensteadt, F. C., & Izhikevich, E. M. (1997). *Weakly connected neural networks*. New York: Springer.

Izhikevich, E. M. (2000). Phase equations for relaxation oscillators. *SIAM Journal on Applied Mathematics, 60*, 1789–1805.

Izhikevich, E. M. (2006). *Dynamics systems in neuroscience: The geometry of excitability and bursting. Chapter 10: Synchronization*. Cambridge: MIT.

Izhikevich, E. M., & Kuramoto, Y. (2006). Weakly coupled oscillators. *Encyclopedia of Mathematical Physics, Elsevier, 5*, 448.

Jones, S. R., Pinto, D., Kaper, T., & Kopell, N. (2000). Alpha-frequency rhythms desynchronize over long cortical distances: A modelling study. *Journal Computational Neuroscience, 9*, 271–291.

Kopell, N. (1988). Toward a theory of modeling central pattern generators. In A. H. Cohen, S. Rossignol, & S. Grillner (Eds.), *Neural control of rhythms*. New York: Wiley.

Kopell, N., Ermentrout, G. B., Whittington, M., & Traub, R. D. (2000). Gamma rhythms and beta rhythms have different synchronization properties. *Proceedings of the National Academy of Sciences of United States America, 97*, 1867–1872.

Kopell, N., & Ermentrout, G. B. (2002). Mechanisms of phase-locking and frequency control in pairs of coupled neural oscillators. In B. Fiedler (Ed.), *Handbook on Dynamical Systems: Toward Applications*. New York: Elsevier.

Kuramoto, Y. (1984). *Chemical oscillations, waves, and turbulence*. Berlin: Springer.

Maran, S. K., & Canavier, C. C. (2008). Using phase resetting to predict 1:1 and 2:2 locking in two neuron networks in which firing order is not always preserved. *Journal of Computational Neroscience, 24*, 37–55.

Mirollo, R. E., & Strogatz, S. H. (1990). Synchronization of pulse-coupled biological oscillators. *SIAM Journal of Applied Mathemaics, 50*, 1645–1662.

Morris, C., & Lecar, H. (1981). Voltage oscillations in the barnacle giant muscle fiber. *Biophysical Journal, 35*, 193–213.

Netoff, T. I., Banks, M. I., Dorval, A. D., Acker, C. D., Haas, J. S., Kopell, N., et al. (2005). Synchronization in hybrid neuronal networks of the hippocampal formation. *Journal of Neurophysiology, 93*, 1197–1208.

Oprisan, S. A., & Canavier, C. C. (2001). Stability analysis of rings of pulse-coupled oscillators: The effect of phase resetting in the second cycle after the pulse is important at synchrony and for long pulses. *Journal of Difference. Equations and Dynamical Systems, 9*, 243–258.

Oprisan, S. A., & Canavier, C. C. (2002). The influence of limit cycle topology on the phase resetting curve. *Neural Computation, 14*, 1027–1057.

Oprisan, S. A., Prinz, A. A., & Canavier, C. C. (2004). Phase resetting and phase locking in hybrid circuits of one model and one biological neuron. *Biophysical Journal, 87*, 2283–2298.

Peskin, C. S. (1975). *Mathematical aspects of heart physiology*. New York: New York University Courant Institute of Mathematical Sciences.

Rinzel, J., & Ermentrout, B. (1998). Analysis of neural excitability and oscillations. In C. Koch & I. Segev (Eds.), *Methods in neuronal modeling: From ions to networks* (2nd edn). Cambridge: MIT.

Rubin, J., & Terman, D. (2000). Geometric analysis of population rhythms in synaptically coupled neuronal networks. *Neural Computation, 12*, 597–645

Sato, Y. D., & Shiino, M. (2007). Generalization of coupled spiking models and effects of the width of an action potential on synchronization phenomena. *Physical Review E, 75*, 011909.

Somers, D., & Kopell, N. (1993). Rapid synchronization through fast threshold modulation. *Biological Cybernetics, 68*, 393–407.

van Vreeswijk, C., Abbott, L. F., & Ermentrout, B. (1994). When inhibition not excitation synchronizes neural firing. *Journal of Computational Neuroscience, 1*, 313–321.

Wang, X. J., Buzsáki, G. (1996). Gamma oscillation by synaptic inhibition in a hippocampal interneuronal network model. *Journal of Neuroscience, 16*, 6402–6413.

White, J. A., Chow, C. C., Ritt, J., Soto-Trevino, C., & Kopell, N. (1998). Dynamics in heterogeneous, mutually inhibited neurons. *Journal of Computational Neuroscience, 5*, 5–16.

Winfree, A. T. (2001). *The geometry of biological time* (2nd edn). New York: Springer.